UNIVERSIDAD DISTRITAL
FRANCISCO JOSÉ DE CALDAS

Ingeniería

https://revistas.udistrital.edu.co/index.php/reving/issue/view/1148

DOI: https://doi.org/10.14483/23448393.19929

Research

Comparative Analysis of Boost and Hybrid Boost Converters

Análisis comparativo entre los convertidores Boost y Boost híbrido

Anamaría Romero Carvajal[1], Nicolás Muñoz-Galeano[1], and Jesús María López-Lezama[1]*

[1]Grupo de Investigación en Manejo Eficiente de la Energía (GIMEL), Departamento de Ingeniería Eléctrica, Universidad de Antioquia (UdeA), Calle 70 No. 52-21, Medellín 050010, Colombia.

Abstract

Context: In power electronics applications, it is important to make comparisons between converters to choose the device that best suits a particular application. This paper compares the Boost converter and the hybrid Boost converter. The operating models of both converters under study are developed and explained in detail to allow for a proper comparison and analysis.

Method: Using the passive sign law, the differential equations that govern the behavior of each converter are determined upon the basis of their switching states. Then, circuit simulations are performed by using the OpenModelica software to analyze the output signals of both converters with the same input parameters.

Results: Comparisons of voltage and current gains, current and voltage time response, and ripple were obtained. Additionally, the efficiency was analyzed by adding resistive losses in each passive element of both converters.

Conclusions: For high duties, the hybrid Boost converter has a greater capacity to increase the output voltage than the Boost converter. It was also found that the hybrid Boost converter has a low overshoot and a low ripple in the time response of its output signals. However, this converter is less efficient.

Keywords: Boost converter, hybrid Boost converter, DC/DC converters, voltage and current gains, efficiency.

Article history

Received: 14th/Sep/2022

Modified: 27th/Dec/2022

Accepted: 14th/Feb/2023

Ing, vol. 28, no. 2, 2023. e19929

*Correspondence: jmaria.lopez@udea.edu.co

Resumen

Contexto: En las aplicaciones de electrónica de potencia, es importante realizar comparaciones entre convertidores para escoger el dispositivo que mejor se adapte a una aplicación en particular. Este artículo compara el convertidor Boost y el convertidor Boost híbrido. Los modelos de operación de ambos convertidores en estudio se desarrollan y explican en detalle para permitir una adecuada comparación y análisis.
Método: Mediante la ley pasiva de signos, se encuentran las ecuaciones diferenciales que rigen el comportamiento de cada convertidor con base en sus estados de conmutación. Acto seguido, se realizan simulaciones circuitales en el *software* OpenModelica para analizar las señales de salida de ambos convertidores con los mismos parámetros de entrada.
Resultados: Se obtuvieron comparaciones de ganancia de voltaje y corriente, respuesta en el tiempo de corriente y voltaje, rizados. Además, se analizó la eficiencia al añadir pérdidas resistivas en cada elemento pasivo de ambos convertidores.
Conclusiones: Para anchos de pulso altos, el convertidor Boost híbrido tiene una mayor capacidad de elevar el voltaje de la salida que el convertidor Boost. También se encontró que el convertidor Boost híbrido presenta bajos sobrepicos y rizados en la respuesta en el tiempo de sus señales de salida. Sin embargo, este convertidor es menos eficiente.

Palabras clave: convertidor Boost, convertidor Boost híbrido, convertidores DC/DC, ganancia de voltaje y corriente, eficiencia.

Table of contents

1. Introduction

DC/DC converters have sparked great interest in power electronics research, as they offer multiple applications in the automotive sector, power amplification, battery energy storage systems, consumer electronics, and communication. These converters allow controlling the DC voltage at the output of a

DC voltage source, acting as energy transfer bridges between sources and loads. There are different boost converter topologies containing a minimum of two semiconductors (a diode and a transistor) and a minimum of one energy storage element (inductor or capacitor). One of the most widely used DC/DC converters in power electronics applications is the Boost converter, given that it offers considerable output voltage gains and high efficiency. For the interconnection of domestic and industrial power with renewable resources, such as photovoltaic (PV) systems, different variations of this converter have been developed, thus leading to hybrid Boost converters, with advantages such as offering higher output voltage gains and improved output signal ripples (1,2).

When studying the behavior of conventional Boost and hybrid Boost converters, as well as conducting comparative analyses, it is necessary to define the converter that best suits an application, with the aim to obtain a high performance. The main objective of this paper is to compare both converters by means of circuit simulations in the OpenModelica software, as well as to present a detailed explanation of their operating principles (3,4).

This paper presents a complete explanation of these converters' modeling, starting from the law of passive signs, when the passive elements of the converter absorb or deliver energy in each switching state. In the literature, it is common to find papers that implement hybrid Boost converter models in different systems without a detailed description of the comprehensive derivation regarding the equations governing the model (5). However, a detailed explanation of the model to be used is of paramount importance for the design of power electronics applications (6–9).

Current research studies have implemented hybrid Boost converter topologies without a precise comparison with conventional Boost converters. Therefore, said comparison is presented in this work to establish the advantages and disadvantages of the Hybrid model (10–13).

The results were obtained by simulating the circuit that allows analyzing the time response of both converters. The OpenModelica software was employed because of its widespread use in the industry, as it is a free and open-source environment based on Modelica. In addition, OpenModelica allows for the simulation of linear and nonlinear systems (14), (15).

The rest of this paper is structured as follows. Section 2 presents the mathematical modeling of the Boost converter. Section 3 presents the mathematical modeling of the hybrid Boost converter. Section 4 corresponds to the results obtained from the simulation of the converter circuits under study. Finally, Section 5 presents the conclusions and analyses derived from this study.

2. Boost converter modeling

Fig. 1 illustrates the topology of the conventional Boost converter under study. This device is composed of the following elements: an input DC voltage source V_i, an inductor L, a switch Q, a diode D, a capacitor C, and a resistive load R.

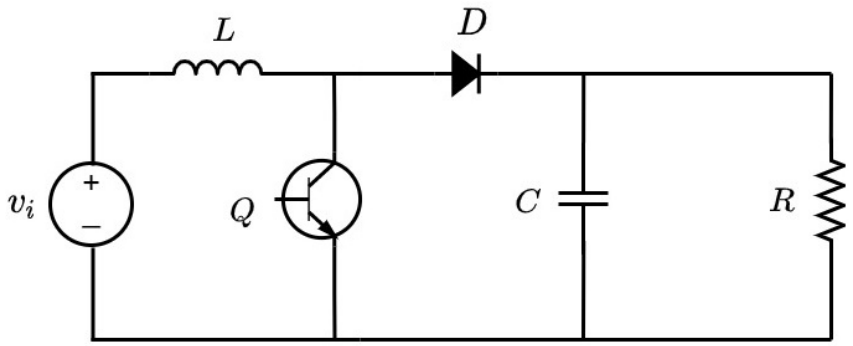

Figure 1. Boost converter topology under study

2.1. Methodology for obtaining voltage and current references

The Boost converter features two switching states, which are depicted in Figs. 2 and 3. In the first state, the switch Q is closed, and the diode has reverse polarity, so the inductor L is in parallel to the source V_i and reacts by absorbing energy, while the capacitor C feeds the resistive load R. In the second state, the switch Q is open while the diode D has direct polarity. Now, the inductor L changes its polarity, and, together with the source V_i, they deliver energy to the capacitor and the load R.

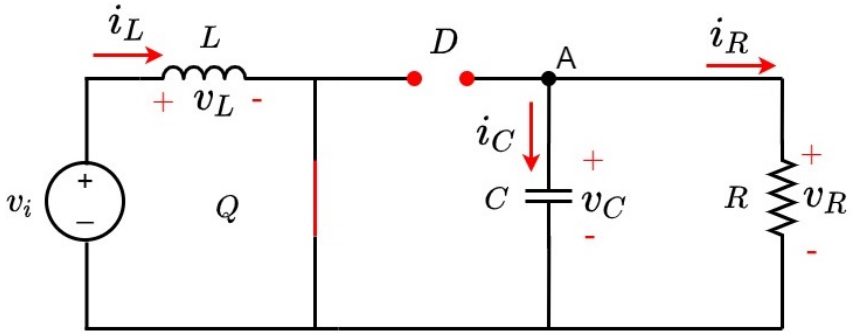

Figure 2. Boost converter with Q closed

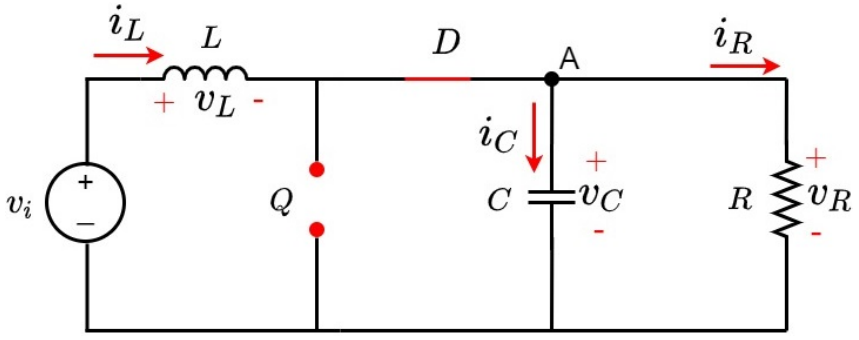

Figure 3. Boost converter with Q open

2.2. Differential equations and switched model

To find the equations that govern the converter's behavior, the differential equations for each switching state are deduced via Kirchhoff's laws, considering the voltage and current references with respect to node A. Eqs. (1) and (2) refer to when switch Q is closed, while Eqs. (3) and (4) refer to when switch Q is open.

$$L \cdot \frac{di_L}{dt} = v_i \tag{1}$$

$$c \cdot \frac{dv_c}{dt} = \frac{-v_c}{R} \tag{2}$$

$$L \cdot \frac{di_L}{dt} = v_i - v_c \tag{3}$$

$$c \cdot \frac{dv_c}{dt} = i_L - \frac{v_c}{R} \tag{4}$$

Subsequently, the auxiliary variable u is defined to obtain the switched model. Thus, when $u = 1$, switch Q is closed; otherwise, when $u = 0$, switch Q is open. Eqs. (1) and (2) yield Eq. (5) which defines the state of the inductor L as a function of u. On the other hand, Eqs. (3) and (4) yield Eq. (6), which defines the state of the capacitor C as a function of u.

$$L \cdot \frac{di_L}{dt} = v_i \cdot u + (v_i - v_c) \cdot (1 - u) \tag{5}$$

$$c \cdot \frac{dv_c}{dt} = \frac{-v_c}{R} \cdot u + (i_L - \frac{v_c}{R}) \cdot (1 - u) \tag{6}$$

2.3. Average model and system gains

To obtain the steady-state mean values of the converter output signals, it is necessary to use the averaging model. This is done by setting the derivatives of Eqs. (5) and (6) as zero. The average of the signals is defined by the average inductor current L (I_L), the average capacitor voltage c (V_c), and the average value of the function u (D), which is called the *duty cycle*.

$$0 = V_i \cdot D + (V_i - V_c) \cdot (1 - D) \tag{7}$$

$$0 = \frac{-V_c}{R} \cdot D + (I_L - \frac{V_c}{R}) \cdot (1 - D) \tag{8}$$

Eqs. (9) and (10) are obtained by clearing Eqs. (7) and (8), respectively. They refer to the voltage and current gains.

$$\frac{V_c}{V_i} = \frac{1}{1 - D} \tag{9}$$

$$\frac{I_L}{I_R} = \frac{1}{1 - D} \tag{10}$$

2.4. Ripple and continuous condition mode (CCM)

Discretizing Eqs. (1) and (2) while considering $\Delta t = DfsW$ results in the inductor current ripple L, Eq. (11), and the capacitor voltage ripple c, Eq. (12).

$$\Delta i_L = \frac{v_i \cdot D}{2L \cdot f_{SW}} \tag{11}$$

$$\Delta v_c = \frac{V_c \cdot D}{2C \cdot f_{SW} R} \tag{12}$$

When the converter operates in continuous conduction mode, a reduction in electromagnetic interference and an easy control of the device is guaranteed. This occurs if the average inductor current is greater than the inductor current ripple, as shown in Eq. (13), which has been obtained by substituting Eqs. (10) and (11) into $|I_L| > |\Delta i_L|$, where $Kc = \frac{2L \cdot f_{SW}}{R}$ and $K(D) = (1-D)^2 D$.

$$Kc > K(D) \tag{13}$$

By making Eq. (13) zero and using the maximum and minimum criterion of differential calculus, the maximum value of $K(D)$ can be found. The maximum value of $K(D)$ is $0,1481$ at a duty of $D = 0,3337$. Therefore, if the converter has a K_c greater than this value, it will show CCM for any steady-state duty cycle value.

3. Modeling the hybrid Boost converter

Fig. 4 illustrates the topology of the hybrid Boost converter under study. The converter is composed of the following elements: an input DC voltage source v_i, two inductors L_1 and L_2, a switch Q, two diodes D_1 and D_2, three capacitors C_1, C_2 and C_3, and a resistive load R.

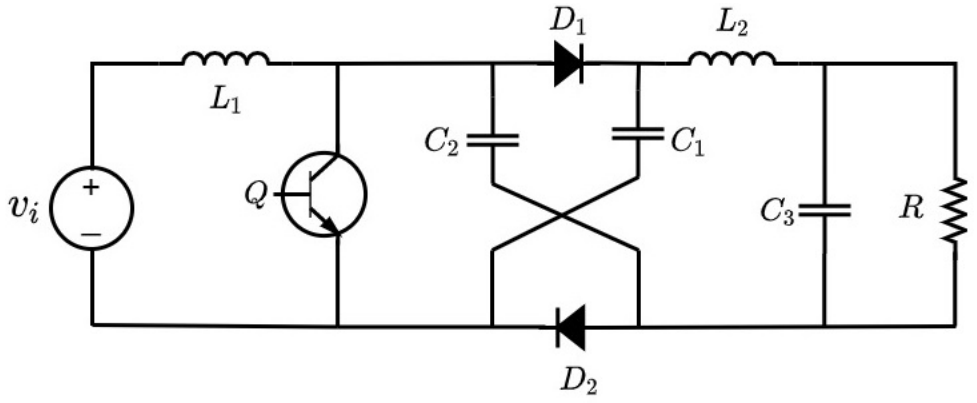

Figure 4. Hybrid Boost converter

3.1. Methodology for obtaining the voltage and current references

The first switching state of the hybrid Boost converter is shown in Fig. 5. In this state, switch Q is closed, so the inductor L_1 absorbs energy by being in parallel to the source v_i. On the other hand, capacitors C_1 and C_2 deliver energy to elements L_3, C_3, and R. This behavior does not allow for the conduction of diodes D_1 and D_2. In the second state, illustrated in Fig. 6, switch Q is open, indicating that inductor L_1, together with source v_i, will now deliver power to capacitors C_1 and C_2, so diodes D_1 and D_2 become directly polarized, and inductor L_3 reacts by delivering power to C_3 and R.

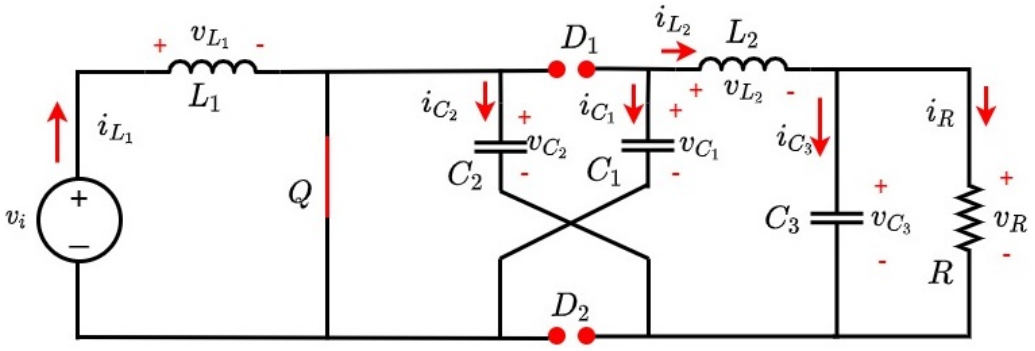

Figure 5. Hybrid Boost converter with Q closed

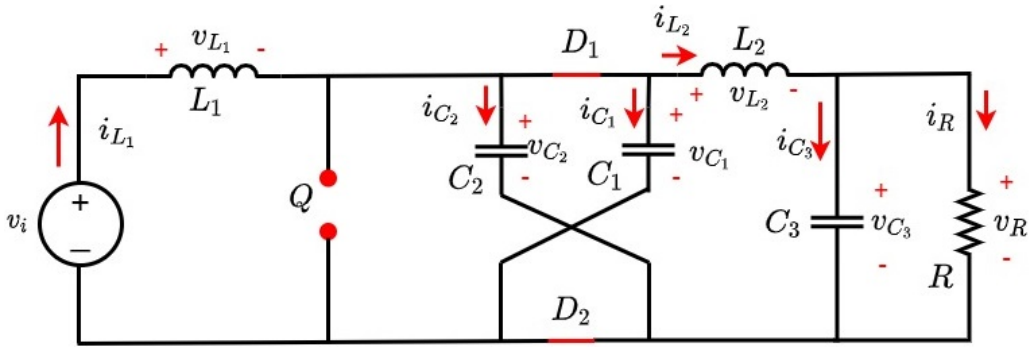

Figure 6. Hybrid Boost converter with Q open

3.2. Differential equations and switched model

The differential equations that govern the behavior of the converter are found using Kirchhoff's laws, considering the voltage and current references at node B and assuming $C_1 = C_2 = C$. Eqs. (14) to (18) refer to when switch Q is closed, while Eqs. (19) (23) refer to when switch Q is open.

$$L_1 \cdot \frac{di_{L_1}}{dt} = v_i \tag{14}$$

$$L_2 \cdot \frac{di_{L_2}}{dt} = 2v_C - v_{C_3} \tag{15}$$

$$C_1 \cdot \frac{dv_{C_1}}{dt} = -i_{L_2} \tag{16}$$

$$C_2 \cdot \frac{dv_{C_2}}{dt} = -\frac{v_R}{R} - C_3 \cdot \frac{dv_{C_3}}{dt} \tag{17}$$

$$C_3 \cdot \frac{dv_{C_3}}{dt} = i_{L_2} - \frac{v_R}{R} \tag{18}$$

$$L_1 \cdot \frac{di_{L_1}}{dt} = v_i - v_{C_1} \tag{19}$$

$$L_2 \cdot \frac{di_{L_2}}{dt} = v_{C_2} - v_{C_3} \tag{20}$$

$$C_1 \cdot \frac{dv_{C_1}}{dt} = i_{L_1} - C_2 \cdot \frac{dv_{C_2}}{dt} - i_{L_2} \tag{21}$$

$$C_2 \cdot \frac{dv_{C_2}}{dt} = i_{L_1} - C_1 \cdot \frac{dv_{C_1}}{dt} - i_{L_2} \tag{22}$$

$$C_3 \cdot \frac{dv_{C_3}}{dt} = i_{L_2} - \frac{v_R}{R} \tag{23}$$

The auxiliary variable u is defined to conveniently write the DEs. When $u = 1$, Q is closed; otherwise, when $u = 0$, Q is open. Eqs. (14) and (19) yield Eq. (24), which defines the state of inductor L_1; Eqs. (15) and (20) yield Eq. (25), which defines the state of inductor L_2; Eqs. (16) and (21) yield Eq. (26), which represents the state of capacitor C_1; Eqs. (17) and (22) yield Eq. (27), which refers to the state of capacitor C_2; and, finally, Eqs. (18) and (23) yield Eq. (28), which defines the state of capacitor C_3.

$$L_1 \cdot \frac{di_{L_1}}{dt} = v_i \cdot u + (v_i - v_{C_1}) \cdot (1 - u) \tag{24}$$

$$L_2 \cdot \frac{di_{L_2}}{dt} = (2v_{C_2} - v_{C_3}) \cdot u + (v_{C_2} - v_{C_3}) \cdot (1 - u \tag{25}$$

$$C_1 \cdot \frac{dv_{C_1}}{dt} = -i_{L_2} \cdot u + (i_{L_1} - C_2 \cdot \frac{dv_{C_2}}{dt} - i_{L_2}) \cdot (1 - u) \tag{26}$$

$$C_2 \cdot \frac{dv_{C_2}}{dt} = (-\frac{v_R}{R} - C_3 \cdot \frac{dv_{C_3}}{dt}) \cdot u + (i_{L_1} - C_1 \cdot \frac{dv_{C_1}}{dt} - i_{L_2}) \cdot (1 - u) \tag{27}$$

$$C_3 \cdot \frac{dv_{C_3}}{dt} = (i_{L_2} - \frac{v_R}{R}) \cdot (u) + (i_{L_2} - \frac{v_R}{R}) \cdot (1 - u) \tag{28}$$

3.3. Average model and system gains

The average of the signals is defined by the average current of the inductors L_1 and L_2 (i_{L_1}, i_{L_2}); the average voltage of the capacitors C_1, C_2, C_3 $(v_{C_1}, v_{C_2}, v_{C_3})$; and the average value of the function u (D), *i.e.*, the duty cycle.

$$0 = V_i \cdot D + (V_i - V_{C_1}) \cdot (1 - D) \tag{29}$$

$$0 = (2V_{C_2} - V_{C_3}) \cdot D + (V_{C_2} - V_{C_3}) \cdot (1 - D \tag{30}$$

$$0 = -I_{L_2} \cdot D + (I_{L_1} - (I_{L_1} + \frac{I_{L_2} - I_{L_1}}{2} - i_{L_2}) \cdot (1 - D) \tag{31}$$

$$0 = (-\frac{V_R}{R} - (\frac{-V_R}{R} + I_{L_2}) \cdot D + (I_{L_1} - \frac{I_{L_2} - I_{L_1}}{2} - i_{L_2}) \cdot (1 - D) \tag{32}$$

$$0 = (I_{L_2} - \frac{V_R}{R}) \cdot (D) + (I_{L_2} - \frac{V_R}{R}) \cdot (1 - D) \tag{33}$$

Eq. (34) indicates the voltage gain, which is obtained from Eqs. (29) and (30), while Eq. (35) refers to the current gain, which is obtained from Eqs. (32) and (33).

$$\frac{V_{C_3}}{V_i} = \frac{1+D}{1-D} \tag{34}$$

$$\frac{I_{L_1}}{I_R} = \frac{1-D}{1+D} \tag{35}$$

3.4. Ripple and continuous condition mode (CCM)

Discretizing Eqs. (14) and (18) with $\Delta t = DfsW$ yields the input current and output voltage ripples given by Eqs. (36) and (37), respectively.

$$\Delta i_{L_1} = \frac{V_i \cdot D}{2L \cdot f_{SW}} \tag{36}$$

$$\Delta v_{C_3} = \frac{i_{L_2} - (\frac{V_{C_3}}{R}) \cdot D}{2C \cdot f_{SW} R} \tag{37}$$

To ensure that the converter operates in continuous conduction mode, the average inductor L_1 current must be greater than the inductor L_1 current ripple. Eq. (38) is obtained by substituting Eqs. (35) and (36) into $|I_L| > |\Delta i_L|$, where $Kc = \frac{2L_1 \cdot f_{SW}}{R}$ and $K(D) = \frac{(1-D)^2 D}{(1+D)^2}$.

$$Kc > K(D) \tag{38}$$

By making Eq. (38) zero and using the maximum and minimum criterion of differential calculus, the maximum value of $K(D)$ can be found. The maximum value of $K(D)$ is $0,0902$ at a duty of $D = 0,2325$. Therefore, if the converter has a K_c greater than this value, it will show CCM for any steady-state duty cycle value.

4. Results

The OpenModelica software (version 1.18) was used to simulate the circuits of both converters. Figs. 7 and 8 show the software implementation of the Boost converter and the Hybrid Boost converter, respectively. These figures show the setpoint block that represents the input voltage of the circuit. Moreover, the pulse block generates a PWM (pulse width modulation) signal that, together with a voltage source, feeds the switch.

Fig. 9 shows the voltage gain *vs.* the duty of the studied converters. The blue signal represents the voltage gain of the Boost converter, while the red signal illustrates the voltage gain of the hybrid Boost converter. It can be seen that, for both converters, the $\frac{Vo}{Vi}$ ratio is proportional to the duty. Furthermore, it is evident that the hybrid Boost converter achieves a higher voltage gain from a duty greater than $10\,\%$, and that, from a duty greater than $85\,\%$, the gain of the hybrid Boost converter almost doubles that of the Boost converter.

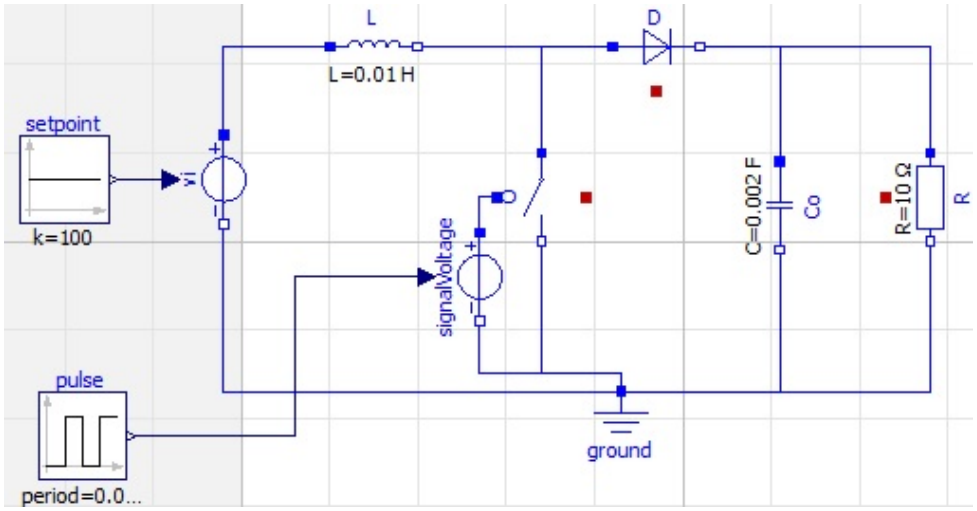

Figure 7. Simulation of the Boost converter in OpenModelica

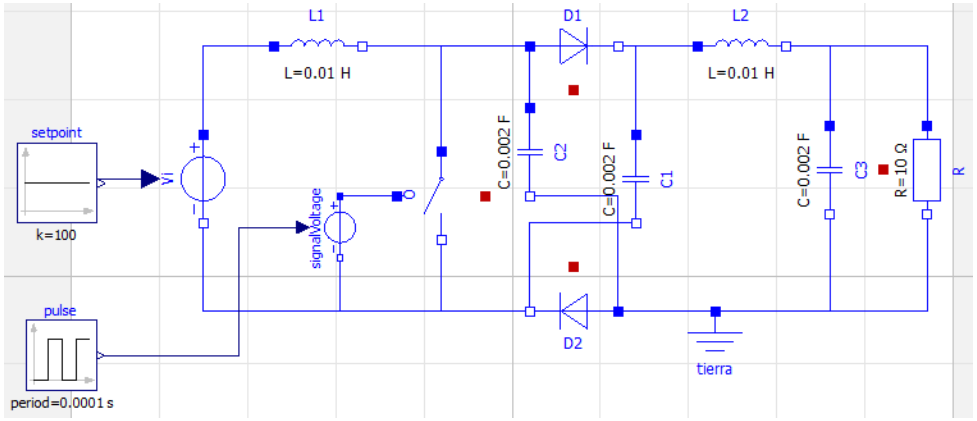

Figure 8. Simulation of the hybrid Boost converter in OpenModelica

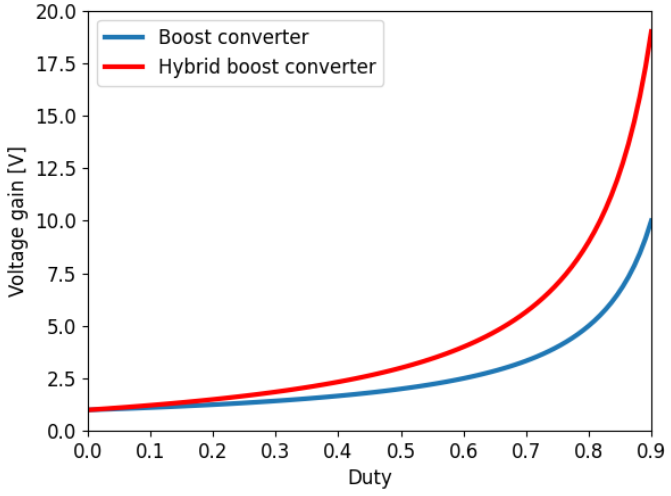

Figure 9. Voltage gain *vs.* duty

The current gain of the converters is illustrated in Fig. 10. The blue signal represents the current gain of the Boost converter, while the red signal illustrates the current gain of the hybrid Boost converter. For both converters, the Io/Ii ratio is inversely proportional to the duty. Furthermore, it is observed that the current gain of the hybrid Boost converter decreases faster for duties below $40\,\%$ than the current gain of the Boost converter. For duties greater than $40\,\%$, as the duty increases, the current gain signal of the hybrid Boost converter begins to decrease at a faster rate than that of the Boost converter. However, the former will always have a lower current gain.

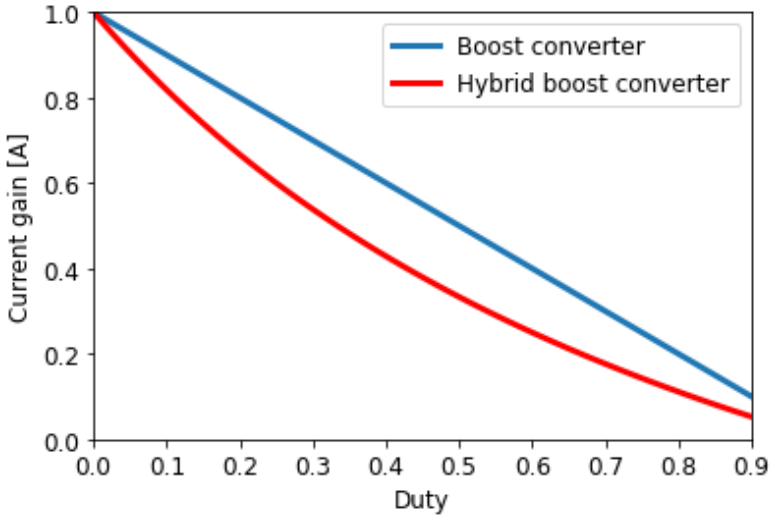

Figure 10. Current gain *vs.* duty

Fig. 11 shows the output voltage (or the voltage across capacitor C or resistor R) and the input voltage Vin of the Boost converter. The green and red signals represents the input and output voltage, respectively. It can be seen that, in the transient state, the output voltage has an overshoot of $50\,\%$ and a settling time of about 0.25 seconds. In a steady state, it has a gain of $100\,\%$ with respect to the input voltage.

As for the hybrid Boost converter, Fig. 12 illustrates the output voltage (or the voltage across capacitor C_3 or resistor R) and the input voltage Vin. The green signal represents the input voltage, and the red signal the output voltage. It is observed that, in the transient state, the output voltage has an over-peak of $45\,\%$ and a stabilization time of approximately 0.45 seconds. In addition, in the steady state, it has a gain of $200\,\%$ with respect to the input voltage.

Fig. 13 shows the output current (or current in the resistor R) and the input current (or current in the inductor L) of the Boost converter. The green signal represents the input current, and the red signal represents the output current. The input current has an overshoot of $150\,\%$ and a settling time of approximately 0.25 seconds. The output current in the transient state has an overshoot of $50\,\%$ and a settling time of approximately 0.22 seconds. In the steady state, it reports a decrease of $50\,\%$ with respect to the input current. Fig. 14 shows the output current (or current at the resistor R) and the input current (or current at L_1) of the hybrid Boost converter. The green signal represents the input current, and the

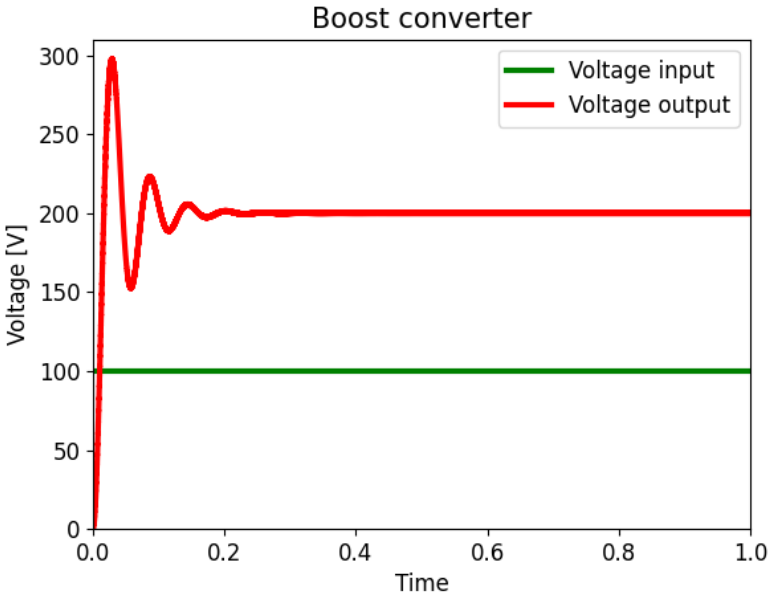

Figure 11. Time response of the voltage in the Boost converter

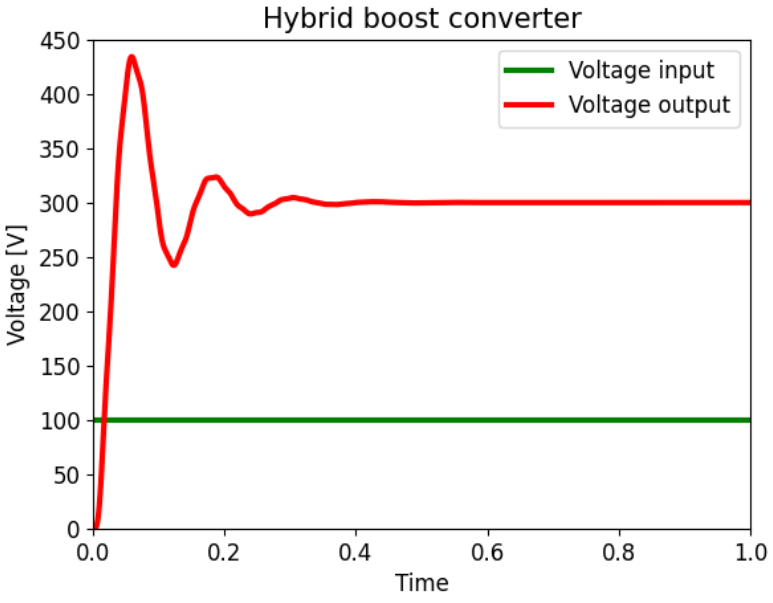

Figure 12. Time response of the voltage in the hybrid Boost converter

red signal represents the output current. It is observed that, in the transient state, the input current presents an over-peak of $122\,\%$ and a settling time of approximately 0.45 seconds. The output current in the transient state has an over-peak of $43\,\%$ and a stabilization time of approximately 0.35 seconds, and it shows a decrease of $33\,\%$ in the steady state with respect to the input current.

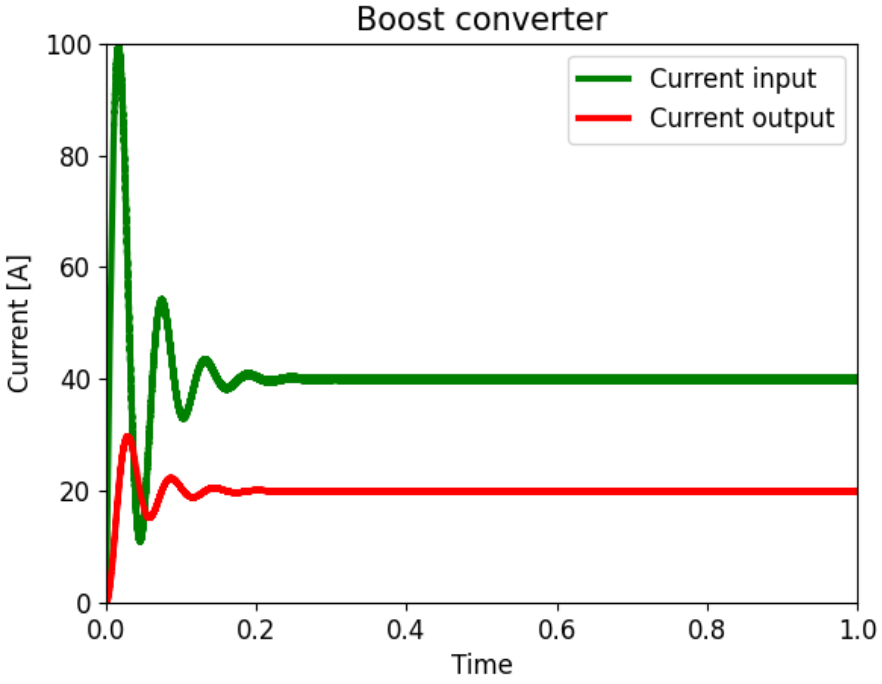

Figure 13. Time response of the current in the Boost converter

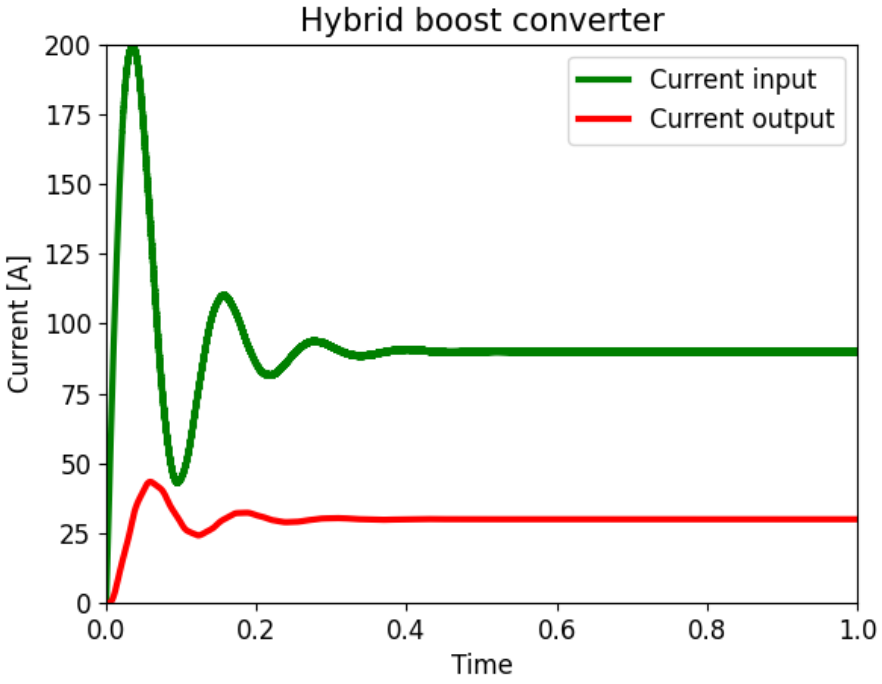

Figure 14. Time response of the current in the hybrid Boost converter

Fig. 15 shows the comparison of the output voltage ripple of the two converters, the red signal refers to the voltage ripple of the Hybrid Boost converter while the orange signal represents the voltage ripple of the Boost converter. The sub-figures in 15 were plotted with the same scale for a proper comparison. The voltage ripple of the Boost converter is $0.5002\ V$, while the voltage ripple of the Hybrid converter is $0.0532\ V$, resulting in a decrease of $840\,\%$.

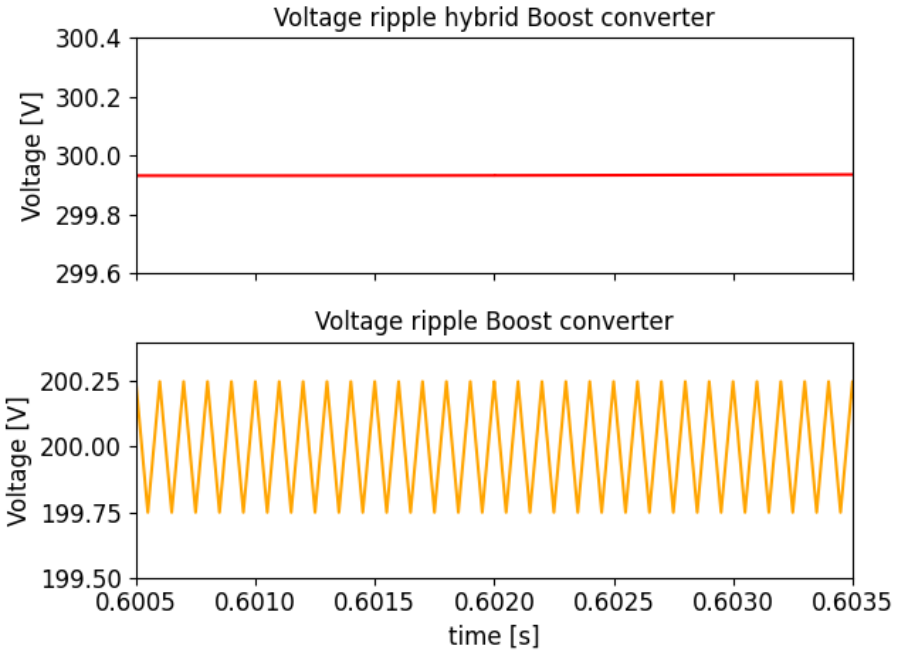

Figure 15. Voltage ripple

Fig. 16 shows a comparison between the output current ripple of the two converters. The red signal refers to the current ripple of the hybrid Boost converter, while the orange signal represents the current ripple of the Boost converter. The sub-figures in Fig. 16 were plotted with the same scale for the sake of comparison. The current ripple of the Boost converter is 0.050, while the voltage ripple of the Hybrid converter is 0.005, which constitutes a $900\,\%$ decrease.

Fig. 17 shows the efficiency with respect to the duty. This was determined by adding the inductor and capacitor losses of $R = 0.3$ in the Open Modelica circuit simulation of both converters. It is observed that, for duties lower than $20\,\%$, the hybrid Boost converter obtains higher efficiency compared to the Boost converter. On the other hand, for duties between 20 and $70\,\%$, the Boost converter manages to a maintain higher efficiency than the hybrid Boost converter. In addition, for duties higher than $70\,\%$, both efficiencies decrease, with a higher efficiency for the Boost converter.

Fig. 18 shows the continuous driving mode for the Boost converter, which is represented by $K(D)\_B$ (blue graph), and for the hybrid Boost converter, denoted by $K(D)\_H$ (orange graph). This comparison is made to illustrate that the Boost converter has less capacity to enter the discontinuous conduction mode, as the maximum value obtained by the KD_B graph is lower than that of the KD_H graph.

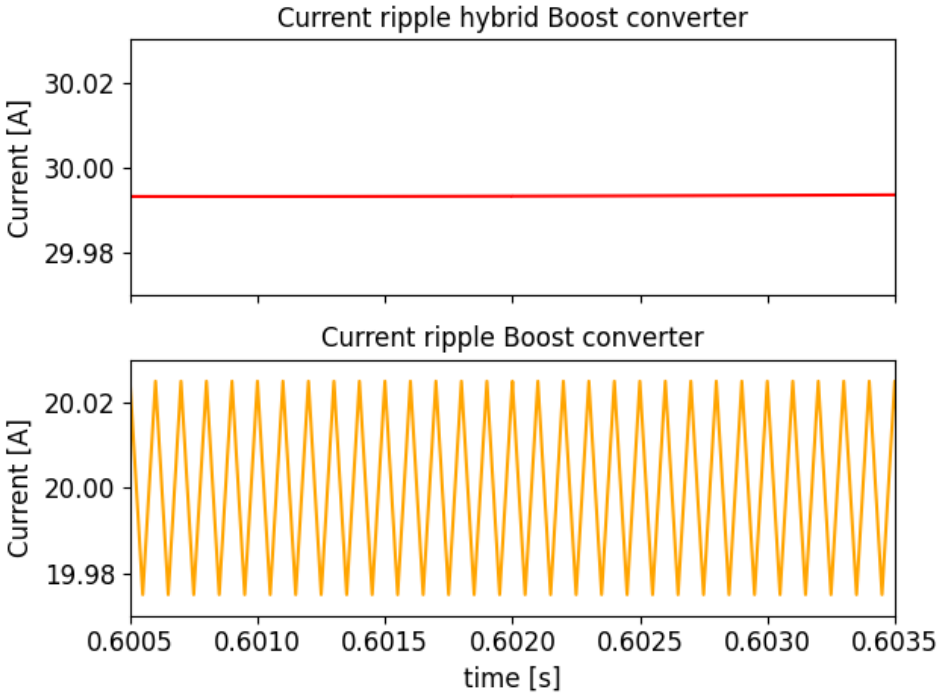

Figure 16. Current ripple

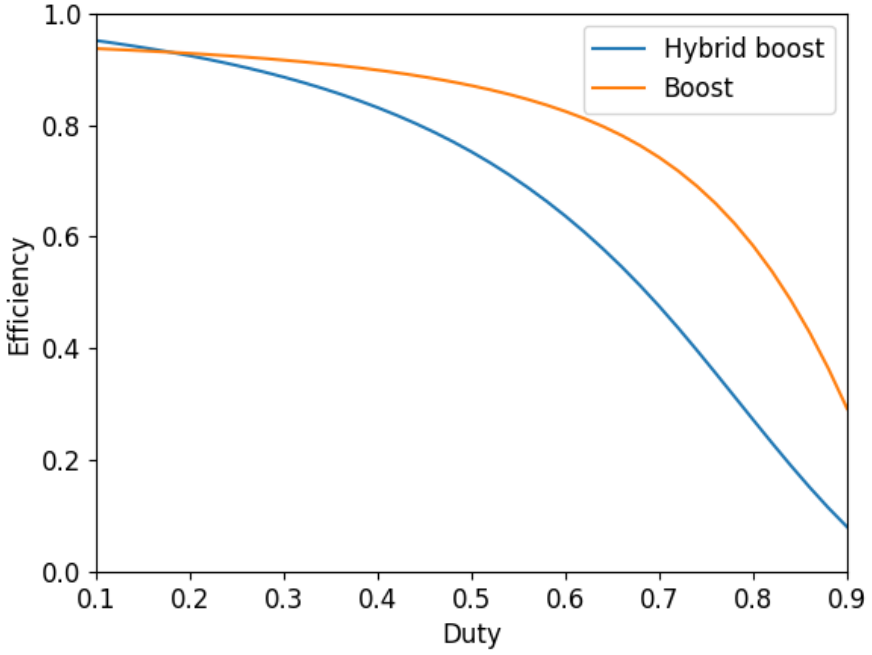

Figure 17. Efficiency

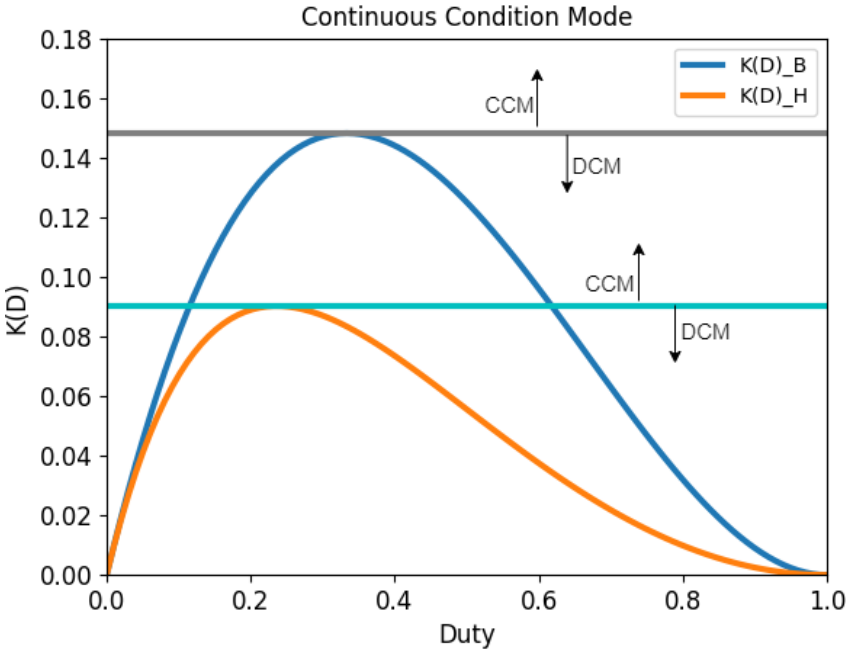

Figure 18. Continuous condition mode

5. Conclusions

This paper presented a comparative analysis of the Boost and hybrid Boost converters. According to the results obtained, it can be stated that, for high voltages, the hybrid converter has a greater capacity to raise the output voltage than the Boost converter. That is because the former has more capacitors in its hybrid branch, which store energy in each switching state. However, for energy conservation at the output, the hybrid Boost converter has a lower current gain than the Boost converter.

For the same input voltage, the hybrid Boost converter has a lower over-peak and a longer output voltage stabilization time than the Boost converter. On the other hand, both converters exhibit different input currents due to the differences in their topologies. The hybrid Boost converter has a higher input current than the other because it has more elements connected in parallel. It can be said that, to work with hybrid Boost converters, having sources whose rated current is higher than the current required by the converter is advised. As for the output current, the Boost converter exhibits less overshoot and less stabilization time than the hybrid Boost converter.

By analyzing the voltage and current ripple, it is concluded that the hybrid Boost converter has much less ripple than the Boost converter. By implementing a hybrid Boost converter, there is an $840\,\%$ decrease in voltage ripple and a $900\,\%$ decrease in current ripple with respect to the Boost converter.

By adding resistive losses of 0,3 Ohms in the inductors and capacitors of both converters, the hybrid Boost converter has a higher efficiency than the Boost converter at voltages below $20\,\%$. For voltages above $20\,\%$, the latter is more efficient than the former, as it has fewer elements and therefore less losses.

6. Contribution of authors

All authors contributed equally to the research.

References

[1] A. Tazay and Z. Miao, "Control of a Three-Phase Hybrid Converter for a PV Charging Station," *IEEE Trans. Energy Convers.*, vol. 33, no. 3, pp. 1002–1014, Sep. 2018. https://doi.org/10.1109/TEC.2018.2812181 3

[2] P. K. Maroti, S. Padmanaban, M. S. Bhaskar, M. Meraj, A. Iqbal, and R. Al-Ammari, "High gain three-state switching hybrid boost converter for DC microgrid applications," *IET Power Electronics*, vol. 12, no. 14, pp. 3656–3667, 2019. https://doi.org/10.1049/iet-pel.2018.6403 3

[3] M. Evzelman and S. Ben-Yaakov, "Modeling and analysis of hybrid converters," in *2012 IEEE Energy Convers. Congr. Expo. (ECCE)*, 2012, pp. 1592–1598. https://doi.org/10.1109/ECCE.2012.6342623 3

[4] B. M. Hasaneen and A. A. E. Mohammed, "Design and simulation of DC/DC boost converter," in *2008 12th Int. Middle-East Power System Conf.*, Mar. 2008, pp. 335–340. https://doi.org/10.1109/MEPCON.2008.4562340 3

[5] B. Axelrod, Y. Berkovich, and A. Ioinovici, "Switched-capacitor/switched-inductor structures for getting transformerless hybrid dc–dc pwm converters," *IEEE Trans. Circ. Syst. I Reg. Papers*, vol. 55, no. 2, pp. 687–696, 2008. 3

[6] D. F. Cortez, M. C. Maccarini, S. A. Mussa, and I. Barbi, "High static gain single-phase PFC based on a hybrid boost converter," *Int. J. Electronics*, vol. 104, no. 5, May 2017. https://doi.org/10.1080/00207217.2016.1253782 3

[7] M. Malik, A. Farooq, A. Ali, and G. Chen, "A DC-DC Boost Converter with Extended Voltage Gain," in *MATEC Web of Conf.*, vol. 40, Dec. 2015. https://doi.org/10.1051/matecconf/20164007001 3

[8] J. C. Rosas-Caro, J. M. Ramirez, F. Z. Peng, and A. Valderrabano, "A DC–DC multilevel boost converter," *IET Power Electronics*, vol. 3, no. 1, pp. 129–137, Jan. 2010. https://doi.org/10.1049/iet-pel.2008.0253 3

[9] F. H. Dupont, C. Rech, R. Gules, and J. R. Pinheiro, "Reduced-Order Model and Control Approach for the Boost Converter With a Voltage Multiplier Cell," *IEEE Trans. Power Electronics*, vol. 28, no. 7, pp. 3395–3404, Jul. 2013. https://doi.org/10.1109/TPEL.2012.2224672 3

[10] S. Belhimer, M. Haddadi, and A. Mellit, "A novel hybrid boost converter with extended duty cycles range for tracking the maximum power point in photovoltaic system applications," *Int. J. Hydrogen Energy*, vol. 43, no. 14, pp. 6887–6898, Apr. 2018. https://doi.org/10.1016/j.ijhydene.2018.02.136 3

[11] Y. Zhang, J.-T. Sun, and Y.-F. Wang, "Hybrid Boost Three-Level DC–DC Converter With High Voltage Gain for Photovoltaic Generation Systems," *IEEE Trans. Power Electronics*, vol. 28, no. 8, pp. 3659–3664, Aug. 2013. https://doi.org/10.1109/TPEL.2012.2229720 3

[12] F. Velasco, S. Casanova, and D. Perez, "Dynamics of a Boost Converter with Inclusion of Internal Resistance Controlled with ZAD." *Rev. Ing. Energética*, vol. 37, no. 2, pp. 144–154, May 2016. 3

[13] M. Evzelman and S. Ben-Yaakov, "Simulation of Hybrid Converters by Average Models," *IEEE Trans. Ind. Appl.*, vol. 50, no. 2, pp. 1106–1113, Mar. 2014. https://doi.org/10.1109/TIA.2013.2272286 3

[14] P. Fritzson, *et al.*, "The OpenModelica Integrated Modeling, Simulation, and Optimization Environment," in *Proc. Amer. Modelica Conf. 2018*, Feb. 2019, pp. 206–219. https://doi.org/10.3384/ecp18154206 3

[15] A. Ganeson, P. Fritzson, O. Rogovchenko, A. Asghar, M. Sjölund, and A. Pfeiffer, "An OpenModelica Python Interface and its use in PySimulator," in *Proc. 9th Int. Modelica Conf.*, Munich, Sep. 2012, pp. 537–548. https://doi.org/10.3384/ecp12076537 3

Anamaría Romero Carvajal

Currently, she is an electrical engineering student and young researcher of the GIMEL research group at Universidad de Antioquia. Her research work is focused on the line of power electronics and control.

Nicolás Muñoz Galeano

He received a BE degree in Electric Engineering at Universidad de Antioquia (UdeA-2004), and a PhD in Electronics Engineering (UPVLC-2011). Since 2005, he has been a professor at the Electric Engineering Department of UdeA (Colombia) and a member of the GIMEL research group. His research work is focused on power electronics design, control, and electrical machines.

Jesús María López Lezama

He received his BSc and MSc degrees from Universidad Nacional de Colombia in 2001 and 2006, respectively. He also received his PhD at Universidade Estadual Paulista (UNESP, SP, Brazil) in 2011. He is currently an associate professor at Universidad de Antioquia, Medellín, Colombia. His main research interests are the planning and operation of electrical power systems and distributed generation